Journal of Thermal Science and Engineering Applications. Received October 29, 2023;
Accepted manuscript posted March 05, 2024. doi:10.1115/1.4065259

A Manuscript Entitled

An Experimental Investigation of Sintered Particle Effect on Heat Transfer Performance in an "Annular Flow" Evaporation Tube

Submitted to

ASME Journal of Thermal Science and Engineering Applications

by

Jeremy Spitzenberger[1], James Hoelle[1], Ahmed Abdulheiba[1] , Ramy H. Mohammed[1], Laith Ismael[1,2], Damena Agonafer[3], Pengtao Wang[4], Stephen Kowalski[4], Kashif Nawaz[4] , Hongbin Ma[1*]

[1] Department of Mechanical & Aerospace Engineering,

University of Missouri, Columbia, MO

[2] Department of Mechanical Engineering

University of Technology, Baghdad, Iraq

[3] Department of Mechanical Engineering, University of Maryland, College Park, MD

[4]Building Technologies Research and Integration Center (BTRIC)

Oak Ridge National Laboratory, Oak Ridge, TN

*Please address all correspondence to:

Hongbin Ma
Professor
Department of Mechanical and Aerospace Engineering
University of Missouri
Columbia,
Tel: 5732394904
Email: mah@missouri.edu

Journal of Thermal Science and Engineering Applications. Received October 29, 2023;
Accepted manuscript posted March 05, 2024. doi:10.1115/1.4065259

ABSTRACT

Wicking structures have been widely used within passive heat transfer devices with high heat fluxes, such as heat pipes, to enhance their thermal performance. While wicking structures promote capillary pumping of the working fluid enhances and thin film evaporation, they can result in capillary evaporation and further enhance the evaporation heat transfer. In this study, a 0.5 mm thick layer of 105 μm sintered copper particles was added to the inner wall of a copper tube, aiming to form an "annular flow" and enhance the heat transfer characteristics by taking advantage of thin film and capillary evaporation. Acetone was chosen as the working fluid, and the performance of an evaporation tube was tested for power inputs of 10, 30, 50, and 70 W. For each power input, trials were run at inclination angles varying from -90° to 90° to investigate the capillary effects. The temperature measurements showed the temperature distribution along the evaporation tube is always downward sloping, meaning the temperature at the fluid inlet is larger than the outlet. Results show that an "annular flow" formed by a thin layer of sintered particles can promote thin-film and capillary evaporation and, therefore, boost the evaporation heat transfer coefficient.

Keywords: copper sintered particles, evaporation, heat transfer

Journal of Thermal Science and Engineering Applications. Received October 29, 2023;
Accepted manuscript posted March 05, 2024. doi:10.1115/1.4065259

1. Introduction

Passive heat transfer devices have gained serious traction in recent years due to their ability to efficiently transfer heat. Improving passive heat transfer in devices such as heat pipes has been at the forefront of research today. A current topic of interest is how wicking structures affect the heat transport capability in passive heat transfer systems. Wicking structures have long been implemented within heat pipes to return working fluid to the evaporating section and utilizing wicking structures to enhance thin film evaporation which can improve evaporative heat transfer coefficients and critical heat fluxes. Hanlon and Ma [1] investigated the sintered particle effect on the capillary flow and thin film evaporation and found that thin film evaporation plays an important role in the enhancement of evaporating heat transfer, and evaporation occurring at the top surface, where the thin film regions were optimized, could reach the maximum evaporating heat transfer coefficient. Bigham and Moghaddem [2,3] investigated the wick structure effect on the flow boiling in a microchannel. The experimental studies deconstruct the boiling heat transfer process into basic heat transfer mechanisms, confirming bubble growth contributes to thin film evaporation in the overall heat transfer of the device. Palko et al. [4] experimentally studied the effects of a porous copper microchannel in conjunction with micromachined heat sinks for high heat flux (>1 kW/cm^2) applications in electronics. It was determined the porous copper structure enhanced the evaporative heat transfer due to improved thin film evaporation on the wicking structure. Plawsky et al. [5] compiled results and conclusions from the 2013 International Workshop on Micro- and Nanostructures for Phase-Change Heat Transfer on thin-film evaporation. It was concluded that thin film evaporation enhances many heat transfer processes, which include energy conversion, microelectronics cooling, boiling, perspiration, and self-assembly operations. It was also noted

Journal of Thermal Science and Engineering Applications. Received October 29, 2023;
Accepted manuscript posted March 05, 2024. doi:10.1115/1.4065259

that surface topography, i.e., wicking structures, can drastically enhance vaporization processes and therefore heat transfer capability of the device.

Thome [6] conducted a comprehensive literature review on the boiling mechanisms within a microchannel. The compiled analytical and experimental results show that the dominant heat transfer mechanism is evaporating thin films around elongated bubbles. Results showed that macroscale models do not represent the heat transfer mechanisms properly but should rather focus on the transient thin film evaporation. Liquid rewetting in microchannels is crucial in ensuring thin film evaporation at the elongated bubbles. Xu et al. [7] experimentally measured the effects of the rewetting process within a microchannel. As the microchannel became partially or completely dried out, the heat transfer capability of the device significantly decreased. By rewetting the device, bubble nucleation occurred, which promoted thin film evaporation, and the overall heat transfer ability of the device was improved. Wang et al. [8] experimentally showed that liquid rewetting of the microchannel induced bubble nucleation, growth, and coalescence, which prompted transient flow and enhanced heat transfer. Dupont et al. [9] proposed a heat transfer model describing the heat transfer capability of a liquid slug, an evaporating elongated bubble, and a vapor slug. The model supports that heat transfer is enhanced due to the evaporating thin film and the importance of proper rewetting to prevent dryout and, thus, the loss of the evaporating thin film. Kandlikar et al. [10] proposed a flow boiling configuration with open microchannels and either a uniform or tapered manifold. The presence of the manifold produced more surfaces for bubble nucleation while reducing backflow due to bubble nucleation and preventing bubble nucleation from drying out areas on the heated surface which led to a dramatic improvement in heat transfer performance.

Dai et al. [11] developed a micromembrane using a single layer of a sintered copper mesh screen to enhance evaporation. The group experimentally determined that adding the

micromembrane enhanced the evaporating surface and improved the critical heat flux by 83% and 198% when compared to microchannels and copper woven mesh laminates, respectively, under similar design and operating conditions. Zhang et al. [12] conducted a visualization study on phase change within a microgrooved heat pipe with evaporation driven by gravity-capillary-forces. It was found that the corner-film evaporation occurring in the rectangular microgrooves improves the overall phase change evaporation performance. Wang et al. [13] applied an aluminum High-Temperature Conductive Microporous Coating (Al-HTCMC) onto an aluminum surface. The coating consisted of aluminum particles brazed onto the aluminum surface, and it was concluded from evaporation experiments that the coating effectively improved wicking capabilities and that the system required almost zero superheat for evaporation to begin on the surface.

Since wicking structures are capable of aiding the heat transfer performance of a device, it is desired to optimize the wicking structure for maximum evaporation. The main factor affecting heat transfer enhancement is the particle size used in the fabrication of the wicking structure. The primary effect particle size has on evaporation is tied to the role that thin film evaporation plays. Comprehensive theoretical, experimental, and simulation studies have been conducted on the thin film evaporating region, and it is established that thin film evaporation greatly improves heat transfer performance during phase change heat transfer. Compared to the boiling heat transfer coefficient on the same surface, the heat transfer coefficient due to thin film evaporation is much higher overall. The reason for this stems from the reduced superheat and the vapor resistance to the liquid film in pool boiling systems.

As shown in Figure 1, the thin film evaporation process for a sintered particle structure can be broken down into three distinct regions/processes: the meniscus film region, the evaporating thin film region, and the non-evaporating region. Within the thin film, a disjoining pressure is

Journal of Thermal Science and Engineering Applications. Received October 29, 2023;
Accepted manuscript posted March 05, 2024. doi:10.1115/1.4065259

created, thus reducing the saturated vapor pressure through the repulsive force and causing easier evaporation and a more efficient heat transfer when heat is added to the thin film region. It is important to note that thin film evaporation isn't exclusive to sintered particles but other geometries and configurations as well.

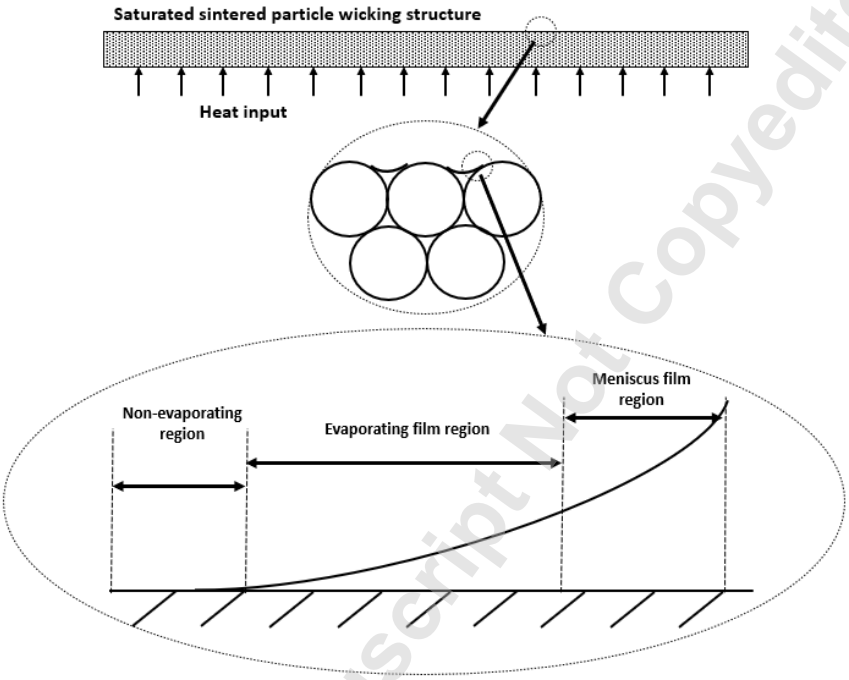

Figure 1: Thin film evaporation in sintered particles.

Hanlon and Ma [1] presented a two-dimensional model to predict the overall heat transfer capability for a sintered wick structure. Results show that thin film evaporation occurring only at the top surface of a wick plays an important role in the enhancement of evaporating heat transfer and the overall heat transfer performance depends on the thin film evaporation, the particle size, the porosity, and the wick structure thickness. Decreasing the average particle radius can enhance the evaporation heat transfer coefficient. Additionally, there exists an optimum characteristic thickness for maximum heat removal. Demsky and Ma [14] proposed a mathematical model to predict evaporating thin film region's evaporation and fluid flow characteristics. The model

predicted thin film evaporation occurring on curved surfaces and showed that the meniscus radius affects the evaporation heat transfer coefficient. Kobayashi et al. [15] conducted theoretical and experimental studies on thin film evaporation at the meniscus edge in an evaporator. The studies agreed with each other and showed that large amounts of heat flux are transported through the thin film region. Ma et al. [16] developed a mathematical model for the evaporating thin film region by considering inertial force, disjoining pressure, surface tension, and curvature. It is determined the inertial force can be neglected, and a maximum velocity, curvature, and heat flux can be selected for optimal enhancement of heat transfer in the evaporating thin film. Nazari et al. [17] studied thin film evaporation in nanochannels and proposed a design for thermal management technologies. The design improved the momentum transport of the liquid, which is the limiting factor in steady-state capillary-driven evaporation. The results showed unprecedented heat fluxes during steady-state conditions over an extended period.

As stated above, the enhancement can be done by introducing sintered particles to the inner wall of a heat pipe or other heat transfer device. As noted by Li and Joshi [18], the sintered particles act as a wicking structure, forcing capillary flow within the tube and also improving thin film evaporation. As seen in the zoomed-in portion of the sintered particles in Figure 1, a thin film evaporates region exists between each set of sintered particles. As a result, adding the sintered particle-wicking structure provides more thin film regions for thin film evaporation to occur, thus improving overall evaporation. When the particle becomes smaller, it can help to increase the thin film regions and enhance the evaporation heat transfer at the liquid-vapor interface. However, reducing particle size may not further enhance the boiling heat transfer in wick structures. Wen et al. [19] conducted an examination of meniscus radii and determined that it is not desirable to make the sintered particle size as small as possible to create the most nucleation sites for bubble

formations to occur. In addition, when determining the sintered particle size, liquid rewetting of the entire capillary structure must be examined. Liquid rewetting is important within capillary-driven flow because too much fluid will cause oversaturation of the sintered particle wicking structure, and no thin film regions will exist, thus causing poor evaporation. If too little fluid is within the wicking structure, the working liquid will evaporate too fast, and burnout or hot spots will occur within the tube walls. As a result, selecting a sintered particle size that will allow for enough fluid flow through the wicking structure while still maintaining evaporating thin films is crucial to enhancing overall evaporation [20]. For flow boiling, however, nucleation sites not only promote thin film evaporation but also initiate the growth of bubbles. To determine the impact of bubble generation, the entire flow regime of a horizontal evaporation tube with a uniform cross-sectional area must be examined, as shown in Figure 2. Fluid flow enters from the left and develops into various regimes as the fluid travels through the evaporation tube, where the heat transfer capability for each region is shown in the plot below the flow regimes. As fluid enters the pipe, nucleation sites produce bubbles that initiate bubbly flow. As more bubbles are formed and further evaporation occurs, the bubbles begin to get bigger and join, producing slug flow within the tube. As slug flow develops, a continuous vapor space is created, and a thin layer of fluid separates the vapor from the tube wall, and annular flow is observed. In the annular flow regime, thin film regions on microgrooved surfaces or a thin layer of sintered particles formed on the tube's inner surface are developed and have a contribution to a spike in the heat transfer coefficient.

Journal of Thermal Science and Engineering Applications. Received October 29, 2023;
Accepted manuscript posted March 05, 2024. doi:10.1115/1.4065259

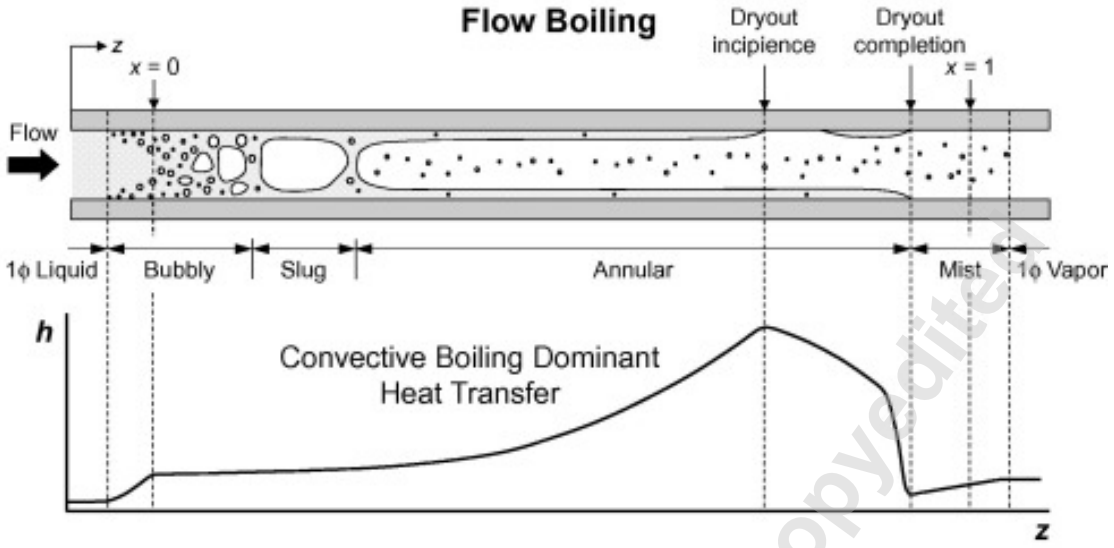

Figure 2: Flow regime and convective heat transfer coefficients for a horizontal tube with uniform circumferential heating [21].

According to the previous discussion, adding a sintered particle wicking structure could improve the overall heat transfer by coupling the capillary-driven flow to thin-film evaporation. Adding sintered particles to the inner tube wall adds more thin film regions for thin film evaporation. In this work, an experimental investigation is performed to investigate the "annular flow" evaporation formed by a thin-layer of sintered particles and the effect of sintered copper particle wicking structure on capillary evaporation in addition to thin film evaporation. An evaporation tube was developed to have evaporation occur at the liquid-vapor interface to study the sintered particle effect on evaporation. The results from this investigation will help to understand how the sintered particles can promote capillary evaporation and thin-film evaporation and, therefore, boost the heat transfer coefficient.

Journal of Thermal Science and Engineering Applications. Received October 29, 2023;
Accepted manuscript posted March 05, 2024. doi:10.1115/1.4065259

2. Experimental Methods

To develop an "annular flow" evaporation and determine the sintered particle effect on the thin film and capillary evaporation, the experimental setup shown in Figure 3 was designed and built. The setup is comprised of a testing section, a reservoir, a condenser, and a collection tank. The testing section consists of a copper tube with an inner diameter of 14 mm and an outer diameter of 15 mm, a 0.5 mm thick layer of 105 μm sintered particles on the inner surface, and a flexible heater wrapped around the outer surface of the copper tube. A sintered particle plug was placed at the entrance region of the evaporation tube to ensure that acetone flows through the sintered wick structures only, as shown in Figure 4. 105 μm was chosen as it is a typical particle size used in heat pipes for electronic cooling.

.

Journal of Thermal Science and Engineering Applications. Received October 29, 2023;
Accepted manuscript posted March 05, 2024. doi:10.1115/1.4065259

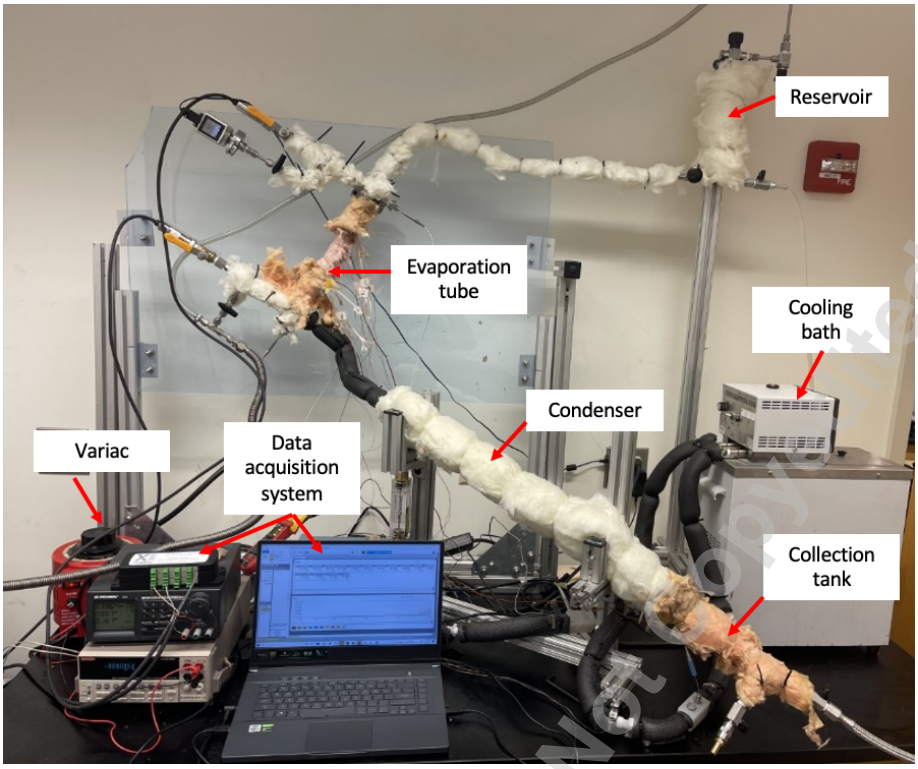

Figure 3: Photo of the experimental setup

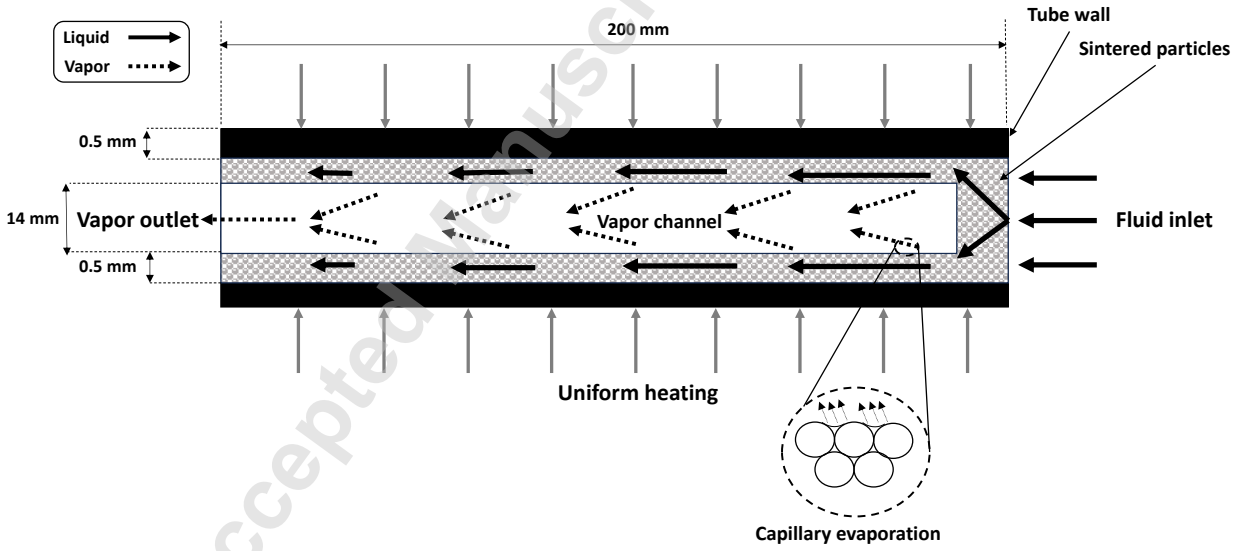

Figure 4: Fluid flow through the evaporation tube test section.

To measure the temperature profile, 11 type-T thermocouples, with an accuracy of ± 0.5 °C, were equally spaced 1.42 cm apart along the outer surface of the evaporation tube. Small grooves

Journal of Thermal Science and Engineering Applications. Received October 29, 2023;
Accepted manuscript posted March 05, 2024. doi:10.1115/1.4065259

were scored into the surface to ensure the thermocouples made good contact with the copper. The thermocouples were then secured using low-resistance thermal epoxy and thermal tape. The epoxy was then used to secure a copper mesh over the thermocouples, and zip-ties were used to hold the mesh in place as the epoxy dried. The copper mesh was applied to ensure more uniform heating across the evaporation tube to minimize hot spots. The heating wrap was then placed around the entire tube and secured with thermal tape to ensure good contact. Finally, insulation was added to the evaporation tube to improve the insulation and reduce the heat losses.

The reservoir serves as the acetone supply while running the trials. Before trials are run, the reservoir is emptied, and then charged with acetone. While conducting a trial, the acetone runs from the reservoir, through a hose, and into the single evaporation tube. As a result, the bottom of the reservoir must be located above the entrance of the single evaporation tube, so gravity can be utilized to promote fluid flow from the reservoir into the evaporation tube. The condenser was connected to a cooling bath at 15° C. As the evaporated acetone vapor leaves the evaporation tube and enters the condenser, the vapor is condensed back to liquid form within the condenser. Finally, a collection tank was connected to the end of the condenser to hold the acetone re-produced in the condenser.

For the experimental procedure to occur, it is crucial that the evaporation tube and the system can hold a vacuum. All experiments must be performed under a vacuum. Assuming the system is properly constructed with no air leaks, the experimental procedure is as follows:

1) Set the evaporation tube to the desired angle for experimentation.
2) Turn on the vacuum pump to begin evacuating the entire system of air.
3) Once vacuum conditions are reached, close the valve on the top of the reservoir, which is connected to the vacuum pump.

Journal of Thermal Science and Engineering Applications. Received October 29, 2023;
Accepted manuscript posted March 05, 2024. doi:10.1115/1.4065259

4) Fill a beaker with 1000 ml of acetone.
5) Attach a hose to the bottom right side of the reservoir (the inlet), which is closed off with a ball valve.
6) Insert the other end of the hose into the beaker filled with 1000 ml of acetone and open the reservoir inlet ball valve. The vacuum created within the reservoir will create a suction effect and pull the acetone from the beaker into the reservoir.
7) Once it appears that no more acetone is being drawn into the reservoir, close the reservoir inlet ball valve. Measure the amount of acetone that is leftover, including the acetone that remains in the hose.
8) Briefly open the valve at the top of the reservoir to remove any air that might have entered the reservoir during the charging process. Close the valve after the excess air has been removed.
9) Once closed, ensure the system is under vacuum conditions, close the valve that separates the vacuum pump from the entire system and turn the vacuum pump off.
10) Using the Variac connected to the heating wrap engulfing the evaporation tube, begin heating the evaporation tube. Allow for a five-minute pre-heating period.
11) Once pre-heated, open the valve at the bottom left side of the reservoir (the outlet) to allow the charged acetone to begin flowing through the evaporation tube. Once the valve has been opened, start a new temperature log.
12) Allow the system to run for 30 minutes uninterrupted. This constitutes one trial.
13) After 30 minutes, close the reservoir outlet valve and turn off the Variac. Collect the leftover acetone in the reservoir and measure how much acetone was used from the

Journal of Thermal Science and Engineering Applications. Received October 29, 2023;
Accepted manuscript posted March 05, 2024. doi:10.1115/1.4065259

reservoir during the trial. Collect the acetone in the condenser and measure how much liquid was produced.

14) After data has been collected and fluids have been measured, repeat steps 2-14 for the subsequent trial at a new power input.

For this study, the above procedure was repeated for power inputs of 10, 30, 50, and 70 W. Trials were conducted for each of these power inputs at angles of -90°, -60°, -30°, 0°, 30°, 60°, and 90° as shown in Figure 5. It is important to note that when the evaporating tube is oriented at a negative angle, gravity aids in fluid flow. However, when the evaporation tube is oriented at positive angles, the fluid flow is more capillary-driven since flow opposes the direction of gravity.

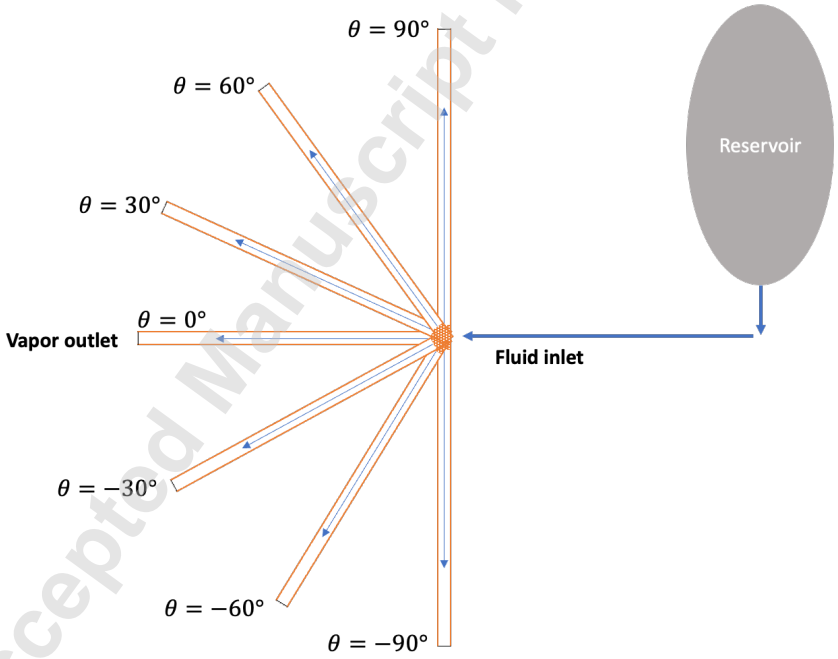

Figure 5: Experimental evaporation tube positions and their corresponding inclination angles.

The power input to the heater can be determined by the voltage and current measurement, i.e. $\dot{Q}_{heater} = I \times V$, where I is the current, V is the voltage. The voltage was measured using the Keithley 2701 digital multimeter with an accuracy of 4% in voltage and current. To calibrate the heat transfer rate added on the tested tubing, the heat transfer rate removed by the condenser is determined by $\dot{Q}_c = \dot{m}_w c_p \left(T_{out} - T_{in}\right)$ where $\dot{m}_w$ is the cooling water mass flow rate, T_{out} is the cooling water outlet temperature, and T_{in} is the cooling water inlet temperature. An energy balance across the entire system was conducted for each trial to estimate heat losses. The power input into the heater, $\dot{Q}_{heater}$, as compared to the heat transfer rate, $\dot{Q}_c$, removed from the condenser and the difference was never found to exceed 6%, indicating the system was well insulated. To ensure the reliability of the experimental results, a few of the trials were repeated three times, and their measured temperature profiles and average steady-state temperatures show that the most significant percent difference in average temperatures was 4.09%, indicating the reliability and repeatability of the results obtained from this experimental investigation.

3. Results and Discussion

The temperature profiles along the evaporation tube are presented for various power inputs and inclination angles to examine the effects of these factors on the heat transfer performance of the evaporation tube. In addition, the working fluid's inlet and outlet temperatures were measured. Table 1 illustrates the wall temperature variation at the power inputs of 30 W, 50 W, and 70 W at a tilted angle of 0 degrees. The microparticles added to the walls had a diameter of 105 μm. When a power input was added on the evaporation tube, liquid flowing in the thin layer of sintered particles vaporized, and the generated vapor flowed through the tube, as shown in Figure 4. With the special design as shown in Figure 4, an “annular flow” evaporation can be formed. Evaporation took place directly at the liquid-vapor-solid interface on the inner surface of the thin layer of

sintered particles, where the superheat for the bubble nucleation and the liquid flow resistance for the bubble flow can be significantly reduced. As shown in Table 1, the outlet temperature of the generated vapor was lower than the inlet temperature of the working fluid. And the wall temperature was typically lower than the inlet temperature of the working fluid. For example, at a power input of 30 W, the fluid inlet temperature was 24.28 °C and the outlet temperature of the generated vapor was 24.04 °C. The outlet temperature of the generated vapor is 0.24 °C lower than the inlet temperature of the working fluid. And the wall temperature is typically lower than the inlet temperature. It demonstrated that the wick structures shown in Figure 4 can readily generate an "annular flow" evaporation producing an extra high heat transfer performance.

Table 1: Average inlet and outlet temperatures and temperature profile of single evaporations tube with Acetone for a tilt angle of 0° and power inputs of 30, 50 and 70 W.

Power Input (W)	Fluid Inlet Temp (°C)	Fluid Outlet Temp (°C)	Wall Temperature (°C)										
			T_1	T_2	T_3	T_4	T_5	T_6	T_7	T_8	T_9	T_{10}	T_{11}
30	24.28	24.04	23.76	36.46	27.24	24.44	33.33	23.81	30.09	23.03	23.84	25.50	25.77
50	24.20	23.97	29.87	50.38	34.44	29.77	44.80	29.21	39.54	28.24	29.60	32.14	32.67
70	24.20	23.99	34.16	62.05	40.22	33.66	54.09	33.02	47.54	32.38	34.41	38.03	38.86

Figure 6 depicts the effect the tilt angle has on the temperature profile on the evaporation tube for a 30 W power input. The corresponding average temperatures for each trial can be observed in Figure 7. From Figure 5, it can be observed that for each corresponding opposite angle, the positive appeared to result in larger surface temperatures. For example, for the tilt angles of -60° and 60°, 60° was found to result in higher surface temperatures. This trend is further backed up by the results of the average steady-state temperatures in Figure 7. For the inclination angles of -30° and 30°, the average steady-state temperatures were 26.89 °C and 27.41 °C, respectively.

Journal of Thermal Science and Engineering Applications. Received October 29, 2023;
Accepted manuscript posted March 05, 2024. doi:10.1115/1.4065259

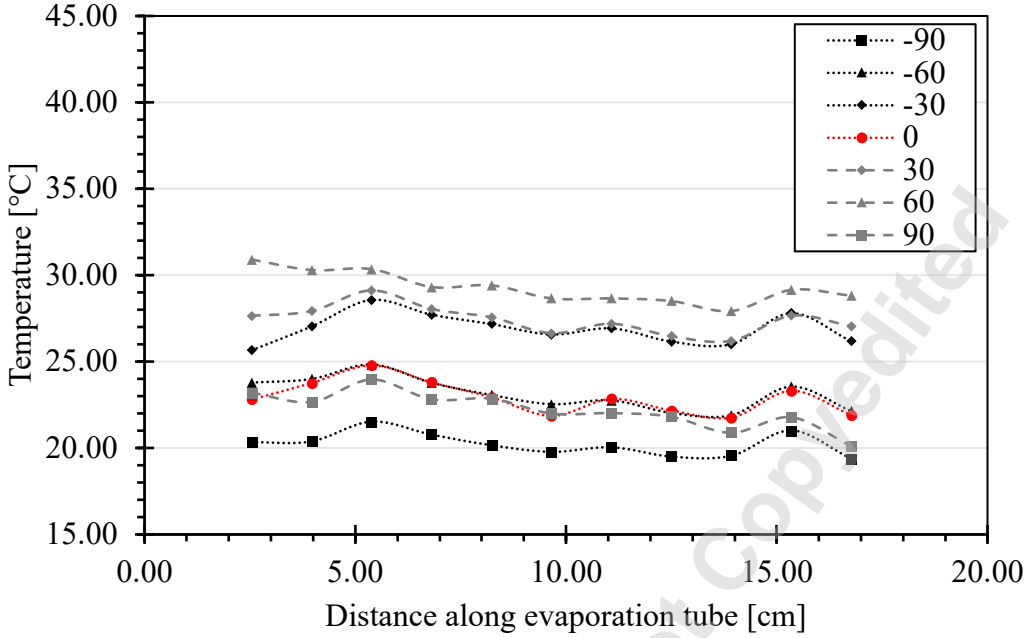

Figure 6: Temperature profile along evaporation tube for a 30 W power input at -90°, -60°, -30°, 0°, 30°, 60°, and 90°.

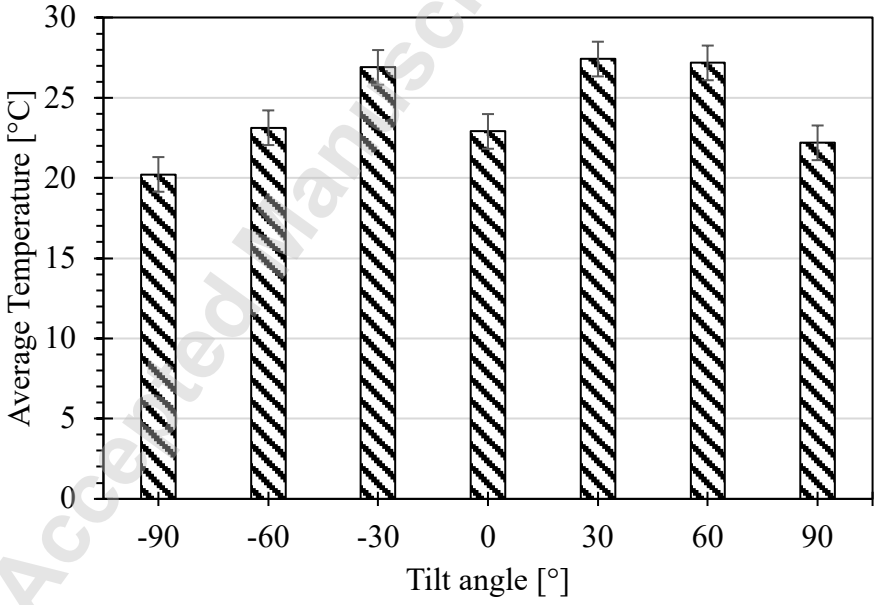

Figure 7*:* Average temperature along the evaporation tube for a 30 W power input.

Journal of Thermal Science and Engineering Applications. Received October 29, 2023;
Accepted manuscript posted March 05, 2024. doi:10.1115/1.4065259

One potential explanation for this is due to the effect of gravity when the evaporation tube is in a negative angle orientation, where the inlet is higher than the outlet. The primary force driving the fluid through the sintered particle wicking structures is capillary force. However, when oriented at a negative angle, the force of gravity is also playing a role which could result in more fluid passing through the tube, thus leading to lower surface temperatures. The results found in Figure 8, which provide a comparison between the total amount of fluid collected in the collection tank for each opposite angle, help to support this theory. On average, the negative angles were observed to produce 60.33 ml more fluid than the positive angles, with the difference between -90°/90° being the largest at 86 ml. It is interesting to note that the angles of -60° and 60° produced the most amount of fluid.

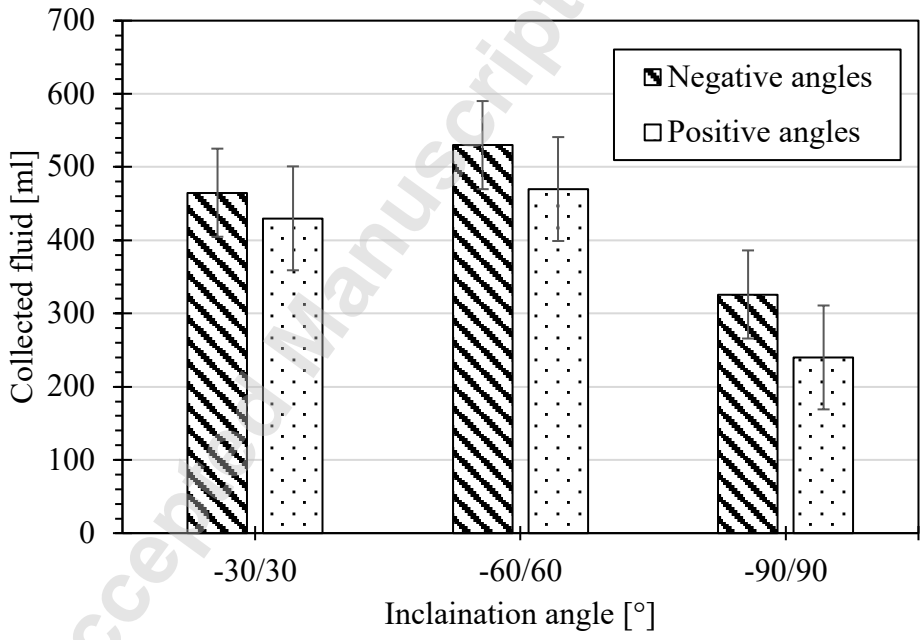

Figure 8: Fluid collected from the collection tank after 30-minute trial.

Journal of Thermal Science and Engineering Applications. Received October 29, 2023;
Accepted manuscript posted March 05, 2024. doi:10.1115/1.4065259

It can also be observed in Figure 6 that the temperature profile along the evaporation tube for all trials was downward sloping, or in other words, the temperature appeared to reduce as the fluid traveled further along the tube. To investigate this trend the inlet and outlet temperatures were compared for each inclination angle for a power input of 30 W, and the results can be observed in Figure 9. As seen in Figure 9, the fluid inlet temperature was always observed to be larger than the outlet temperature, with no exceptions. Clearly it demonstrated that the wick structure shown in Figure 4 can manually generate an "annular flow" evaporation. Another interesting observation that can be made is that larger inclination angles resulted in larger fluid inlet temperatures and consequentially larger outlet temperatures as well. As with the results shown in Figure 7 for the average temperatures, this can also be due to the effect of gravity. The larger the tilt angle, the more the fluid will have to work against gravity. Therefore, the contact time between the fluid and the wall of the inner wall is greater, thus resulting in the fluid being heated to a higher temperature. Similarly, as the results in Figure 8, less fluid is passing through the evaporation tube for larger inclination angles, and therefore, the fluid will be able to reach higher temperatures at the same heat inputs.

Journal of Thermal Science and Engineering Applications. Received October 29, 2023;
Accepted manuscript posted March 05, 2024. doi:10.1115/1.4065259

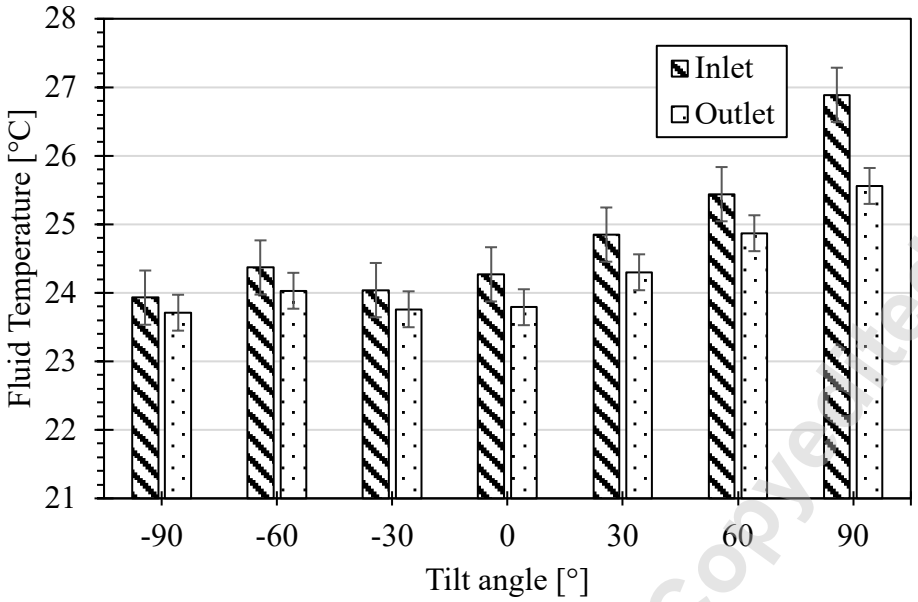

Figure 9: Inlet and outlet temperatures for working fluid for a 30 W power input.

The performance of the evaporation tube was tested at power inputs of 10, 30, 50, and 70 W for each tilt angle. The temperature distribution along the evaporation tube for all heat inputs at a 60° tilt angle can be observed in Figure 10. As would be expected, a larger heat input was typically found to result in larger surface temperatures, as shown by the average temperatures in Figure 11. As with the results shown in Figure 6, the temperature distributions in Figure 10 are all downward sloping. However, the slope appears to be more negative for larger power inputs as opposed to the results in Figure 6, where all trials were for the same 30 W power input, and only the tilt angle was changing. For those trials, the slopes appeared to be very similar, and the temperature distributions followed the same trend. The temperatures distributions for tilt angles -90°, -60°, -30°, 30°, 60°, and 90° for power inputs of 50 W and 70 W were plotted to see if this trend is consistent for other power inputs, and those can be observed in Figure 12 and Figure 13, respectively. From those results, as with the 30 W power input, the temperature distributions for

Journal of Thermal Science and Engineering Applications. Received October 29, 2023;
Accepted manuscript posted March 05, 2024. doi:10.1115/1.4065259

the 50 W and 70 W all appeared to follow similar trends for each tilt angle, with the only main difference being the average temperatures which followed the same trend described in Figure 7.

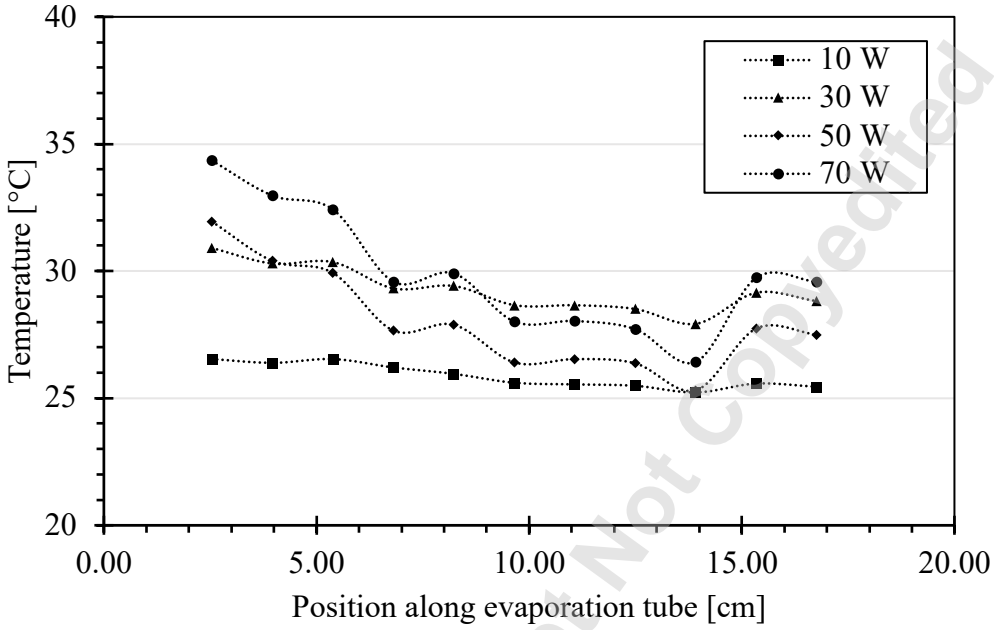

Figure 10: Temperature profile along evaporation tube at 60° for power inputs of 10, 30, 50, and 70 W.

Journal of Thermal Science and Engineering Applications. Received October 29, 2023;
Accepted manuscript posted March 05, 2024. doi:10.1115/1.4065259

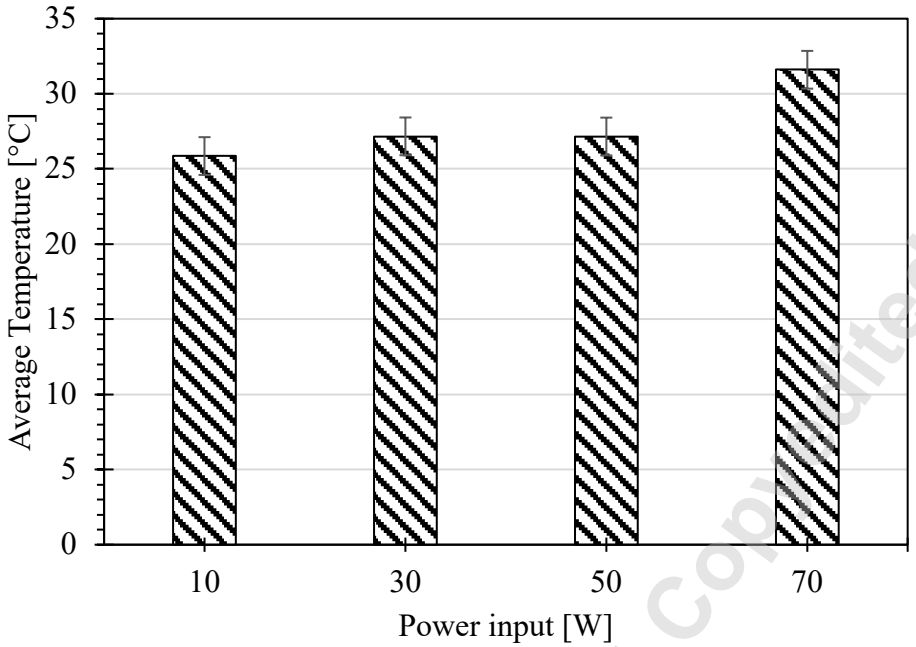

Figure 11: Average steady state temperature for a 60° tilt angle at power inputs of 10, 30, 50, and 70 W.

From Figure 10, the temperature readings from 2–8 cm along the evaporation tube make sense, meaning the higher power inputs resulted in higher temperatures. However, at some point between 8-10 cm, the temperature for the 70 W power input was observed to drop below that of the 50 W power input. It wasn't until around 15 cm where a sharp increase in the temperature of the 70 W mark was observed, and it returned above that of the 50 W. A temperature increase was observed at this location for all power inputs, however, the jump was much more significant at 70 W. As can be seen in Figure 13, this pronounced temperature jump was observed for all tilt angles. This temperature increase could be due to a dryout condition, where all the fluid had been fully evaporated and therefore resulting in higher surface temperatures near the outlet.

Journal of Thermal Science and Engineering Applications. Received October 29, 2023;
Accepted manuscript posted March 05, 2024. doi:10.1115/1.4065259

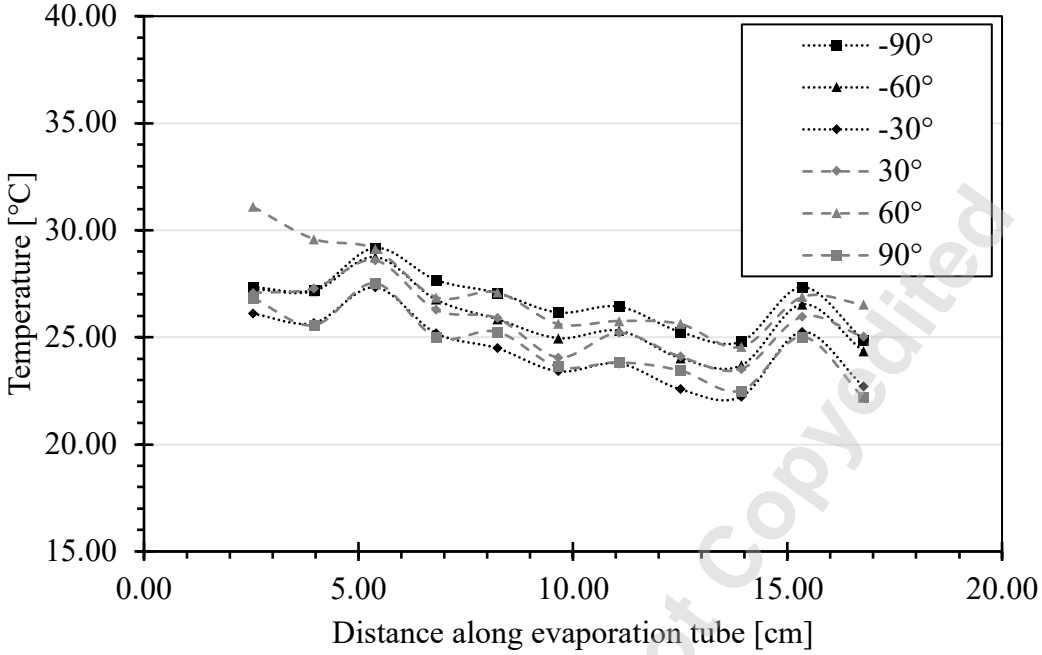

Figure 12: Temperature profile along evaporation tube for a 50 W power input at -90°, -60°, -30°, 30°, 60°, and 90°.

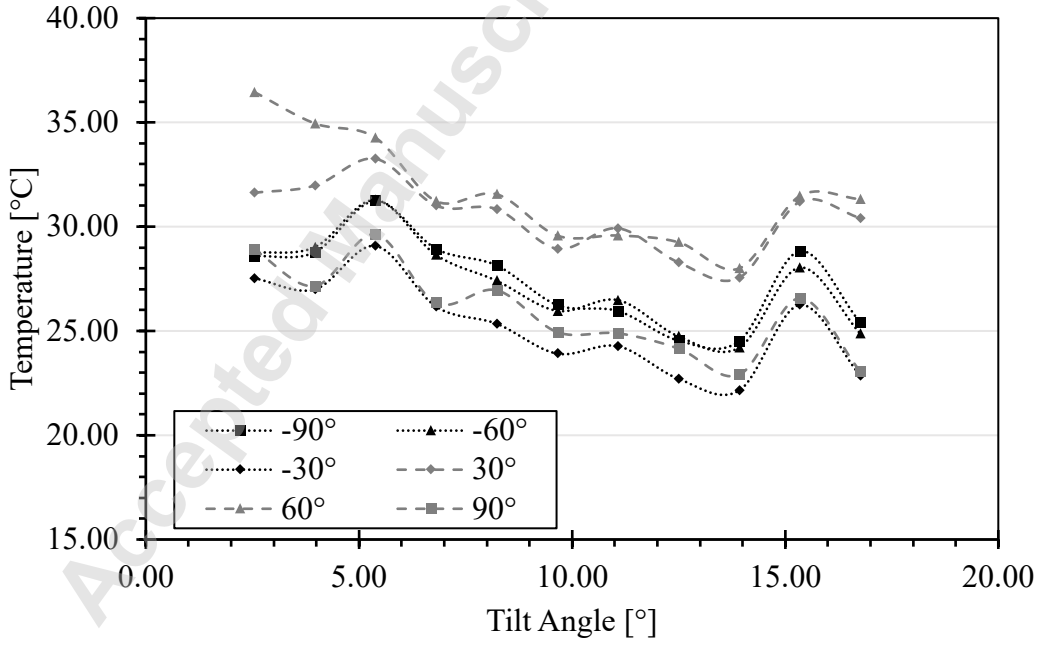

Figure 13: Temperature profile along evaporation tube for a 70 W power input at -90°, -60°, -30°, 30°, 60°, and 90°.

Journal of Thermal Science and Engineering Applications. Received October 29, 2023;
Accepted manuscript posted March 05, 2024. doi:10.1115/1.4065259

The average steady-state temperatures for tilt angles -90°, -60°, -30°, 30°, 60°, and 90° for power inputs of 30 W, 50 W, and 70 W, can be observed in Figure 14. As would be expected, for almost all tilt angles, the larger power inputs resulted in larger average temperatures. The only exceptions to this occurred at -30° and 30°, where for both cases, the 30 W power input resulted in a larger average surface temperature when compared to both 50 W and 70 W at -30°, and 50 W when at 30°. In addition to this, a tilt angle of 90° was observed to result in the lowest average surface temperatures except for 30 W, where it was the second lowest, with -90° being the lowest.

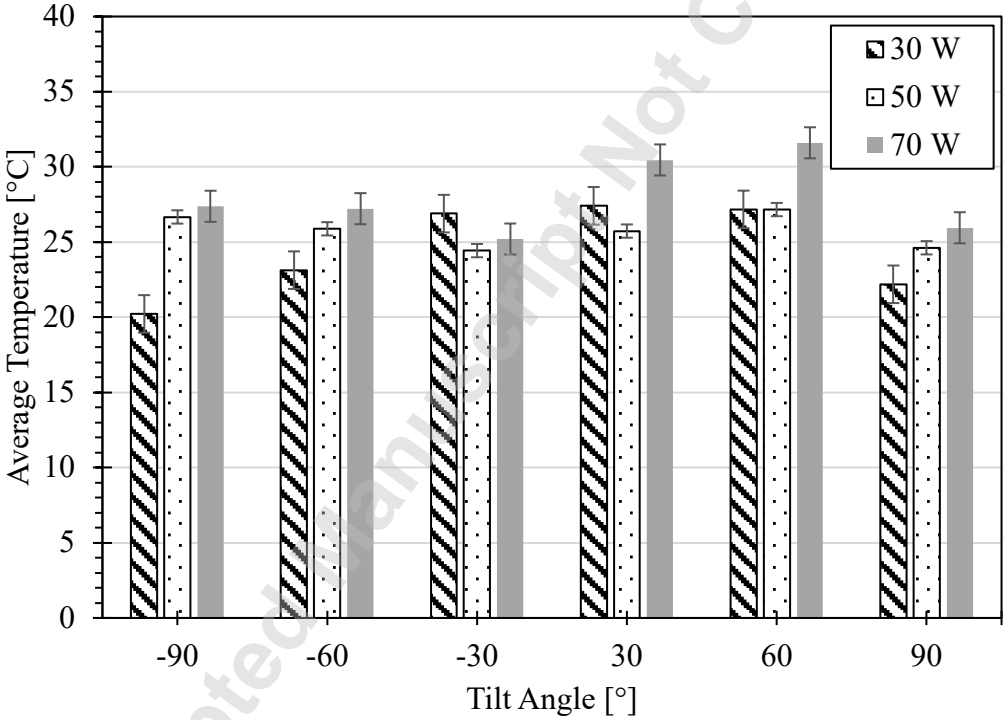

Figure 14: Average temperature along evaporation tube for a 30, 50, and 70 W power input.

The wick structure shown in Figure 4 can produce an “annular flow” evaporation and can enhance the evaporation heat transfer as presented above. In addition, the microparticles can reduce the meniscus radius, which can directly reduce the saturation pressure, and the evaporation

temperature can be further reduced. Ma and Peterson [22] show that the saturation pressure depends on the meniscus radius and electric field in addition to the saturation temperature. If the electric field is zero, the saturation pressure can be further reduced as described by the Kelvin equation, given as [23]

$$p_{sat} = p_o e^{\frac{h_{lv}}{R}\left(\frac{T-T_o}{TT_o}\right)-\frac{2\sigma v_l}{r_e RT}} \quad (1)$$

where p_{sat} is the saturation pressure, p_o and T_o are is a reference pressure and temperature, respectively, h_{lv} is the latent heat, T is the measured temperature, R is the gas constant, σ is the surface tension, ν is the viscosity, and r_e is the meniscus radius. From Eq. (1), it can be found that the saturation pressure depends on the meniscus radius in addition to the saturation temperature. As the meniscus radius decreases, the saturation pressure decreases. Cheng and Ma [24] derived an equation to predict the average meniscus radius at the liquid-vapor interface and found that the average meniscus radius for particle wicks with a uniform radius of r_p, can be found that $r_e = 0.443r_p$ where r_p is the radius of the sintered particle. However, for triangular particle structures, which occurs most frequently, accounting for 45% of the particle structure $r_e = 0.103r_p$ [23]. Based on the particle diameter of 105 μm used in this experimental investigation, a reduction of the evaporation temperature of 0.02 °C can be found for a reference temperature of 30 °C. Clearly, when the particle becomes smaller, the saturation pressure becomes smaller and will further reduce the evaporation temperature.

4. CONCLUSIONS

Utilizing wicking structures created from sintered copper particles added to inner surface and inlet of an evaporation tube, an "annular flow" evaporation can be readily obtained to enhance the evaporation heat transfer. Experimental studies were conducted to study the effect of the sintered

particles on the surface temperature profile of the evaporation tube at heating power inputs of 10, 30, 50, and 70 W and inclination angle ranging from -90° to 90°, with acetone acting as the working fluid. The results from the experimental investigation showed that inclination angles of -30° and 30° resulted in the largest average surface temperatures, whereas experimental studies conducted at inclination angles of -60° and 60° produced more condensate. The power input into the evaporation tube was found to have a greater effect on the temperature distribution along the evaporation tube compared to the inclination angle. For all trials, inlet temperature of the fluid was found to be higher than the outlet temperature of the vapor. Similarly, the temperature distribution along the evaporation tube was always observed to be downwards sloping, with larger power inputs resulting in a steeper slope and at some location the outlet temperature of the fluid was found to be lower than the surface temperature. Results shown that the "annular flow" evaporation investigated herein can enhance the evaporation heat transfer, and while smaller meniscus radius produced by the micro or nanostructured wicks can further increase thin film evaporation, it can further enhance the capillary evaporation by reducing the meniscus radius.

ACKNOWLEDGEMENTS

The work presented in this article was supported by the Office of Naval Research Grant No. N00014-19-1-2006, under the direction of Dr. Mark Spector. This material is based upon work supported by the U.S. Department of Energy, Office of Science, Building Technologies Office. This research used resources of the Building Technologies Research and Integration Center (BTRIC) of the Oak Ridge National Laboratory, which is a DOE Office of Science User Facility.

Declaration of Competing Interests

The authors state that they have no known competing financial interests or personal relationships that could have influenced the work reported in this paper.

REFERENCES

[1] Hanlon, M. A., and Ma, H.B., 2003, "Evaporation Heat Transfer in Sintered Porous Media," ASME Journal of Heat Transfer, 125(4), pp. 644-653.
[2] Bigham, S., and Moghaddam, S., 2015, "Microscale Study of Mechanisms of Heat Transfer during Flow Boiling in a Microchannel," International Journal of Heat and Mass Transfer, 88, pp. 111–121.
[3] Bigham, S., and Moghaddam, S., 2015, "Role of Bubble Growth Dynamics on Microscale Heat Transfer Events in Microchannel Flow Boiling Process," Appl Phys Lett, 107(24), p. 244103.
[4] Palko, J. W., Lee, H., Agonafer, D. D., Zhang, C., Jung, K. W., Moss, J., Wilbur, J. D., Dusseault, T. J., Barako, M. T., Houshmand, F., Rong, G., Maitra, T., Gorle, C., Won, Y., Rockosi, D., Mykyta, I., Resler, D., Altman, D., Asheghi, M., Santiago, J. G., and Goodson, K. E., 2016, "High Heat Flux Two-Phase Cooling of Electronics with Integrated Diamond/Porous Copper Heat Sinks and Microfluidic Coolant Supply," Proceedings of the 15th InterSociety Conference on Thermal and Thermomechanical Phenomena in Electronic Systems, ITherm 2016, pp. 1511–1517.
[5] Plawsky, J. L., Fedorov, A. G., Garimella, S. v, Ma, H. B., Maroo, S. C., Chen, L., and Nam, Y., 2014, "Nano-and Microstructures for Thin-Film Evaporation-A Review," Nanoscale and Microscale Thermophysical Engineering, 18(3), pp. 251-269.
[6] Thome, J. R., 2004, "Boiling in Microchannels: A Review of Experiment and Theory," Int J Heat Fluid Flow, 25(2), pp. 128–139.
[7] Xu, J., Gan, Y., Zhang, D., and Li, X., 2005, "Microscale Boiling Heat Transfer in a Micro-Timescale at High Heat Fluxes," J. Micromech. Microeng, 15, pp. 362–376.
[8] Wang, Y., Wang, P., Wang, N., Pan, Y., Xu, J., Shen, S., Gan, Y., Li, Y., Zhang, W., and Su, Q., 2005, "Transient Flow Pattern Based Microscale Boiling Heat Transfer Mechanisms," Institute of Physics Publishing Journal of Micromechanics and Microengineering, 15, pp. 1344–1361.
[9] Dupont, V., Thome, J. R., and Jacobi, A. M., 2004, "Heat Transfer Model for Evaporation in Microchannels. Part II: Comparison with the Database," Int J Heat Mass Transf, 47(14–16), pp. 3387–3401.
[10] Kandlikar, S. G., Widger, T., Kalani, A., and Mejia, V., 2013, "Enhanced Flow Boiling over Open Microchannels with Uniform and Tapered Gap Manifolds," ASME J Heat Transfer, 135(6), p.061401.
[11] Dai, X., Yang, F., Yang, R., Lee, Y.-C., and Li, C., 2013, "Micromembrane-Enhanced Capillary Evaporation." Appl. Phys. Lett., 103, p. 151602.
[12] Zhang, C., Yu, F., Li, X., and Chen, Y., 2019, "Gravity–Capillary Evaporation Regimes in Microgrooves," AIChE Journal, 65(3), pp. 1119–1125.

[13] Wang, X., Fadda, D., Godinez, J. C., Lee, J., and You, S. M., 2020, "Capillary Evaporation of Water from Aluminum High-Temperature Conductive Microporous Coating," Int J Heat Mass Transf, 153, p. 119660.
[14] Demsky, S. M., and Ma, H. B., 2010, "Thin Film Evaporation on a Curved Surface," Microscale Thermophysical Engineering, 8(3), pp. 285-299.
[15] Kobayashi, Y., Ikeda, S., and Iwasa, M., 2012, "Evaporative Heat Transfer at the Evaporative Section of a Grooved Heat Pipe," AIAA Journal of Thermophysics and Heat Transfer 10(1), pp. 83–89.
[16] Ma, H. B., Cheng, A. P., Borgmeyer, A. B., and Wang, A. Y. X., 2008, "Fluid Flow and Heat Transfer in the Evaporating Thin Film Region," Microfluidics and Nanofluidics, 4(3), pp. 237-243.
[17] Nazari, M., Gorman, M., and Ghasemi, H., 2019, "Unprecedented Capillary Evaporative Heat Flux in Nanochannels," InterSociety Conference on Thermal and Thermomechanical Phenomena in Electronic Systems, ITHERM, May, pp. 329–334.
[18] Li, W., and Joshi, Y., 2020, "Capillary-Assisted Evaporation/Boiling in PDMS Microchannel Integrated with Wicking Microstructures," Langmuir, 36(41), pp. 12143–12149.
[19] Wen, R., Xu, S., Lee, Y.-C., and Yang, R., 2018, "Capillary-Driven Liquid Film Boiling Heat Transfer on Hybrid Mesh Wicking Structures." Nano Energy, 51, pp. 373-382.
[20] Farokhnia, N., Irajizad, P., Sajadi, S. M., and Ghasemi, H., 2016, "Rational Micro/Nanostructuring for Thin-Film Evaporation," Journal of Physical Chemistry C, 120(16), pp. 8742–8750.
[21] Kim, S. M., and Mudawar, I., 2014, "Review of Databases and Predictive Methods for Heat Transfer in Condensing and Boiling Mini/Micro-Channel Flows," Int J Heat Mass Transf, 77, pp. 627–652.
[22] Ma, H. B., and Peterson, G. P., 1995, "Thermodynamic Analysis of the Influence of Electric Fields on Frost Formation," AIAA Journal of Thermophysics and Heat Transfer, 9(3), pp. 562-565.
[23] Ma, H., 2015, Oscillating Heat Pipes, Springer, New York.
[24] Cheng, P., and Ma, H. B., 2007, "A Mathematical Model Predicting the Minimum Meniscus Radius in Mixed Particles," ASME J Heat Transfer, 129(3), pp. 391–394.